JTTEE5 16:744–750
DOI: 10.1007/s11666-007-9075-y
1059-9630/$19.00 © ASM International

Peer Reviewed

Fast Modeling of Phase Changes in a Particle Injected Within a d.c Plasma Jet

F. Ben Ettouil, B. Pateyron, H. Ageorges, M. El Ganaoui, P. Fauchais, and O. Mazhorova

(Submitted March 16, 2007; in revised form July 16, 2007)

When spraying ceramic particles with a low thermal conductivity such as zirconia using Ar-H_2 direct-current (d.c.) plasma jets where the heat transfer is important, heat transfer phenomena take place with the propagation of melting, evaporation and even afterwards solidification fronts. Most models neglect these heat transfer phenomena assuming the particle as a lumped media. This work is aimed at developing a model coupling the effect of heat propagation within the particle along its trajectory. It uses an adaptative grid in which the coordinates of the phase change fronts are fixed. It allows minimizing the calculation costs (approximately 10 s on PC under Windows XP against 1 h with an enthalpy model). Such calculations are illustrated in an Ar-H_2 (25 vol.%) for dense and porous agglomerated zirconia (low thermal conductivity) as well as iron particles with a much higher thermal conductivity and drastic evaporation.

Keywords d.c. plasma spray, fast modeling, nanostructured materials, phase change

1. Introduction

The plasma spraying process has been the subject of numerous numerical modeling, the latest one treating the whole complexity of the physical phenomena by taking into account the arc root fluctuations at the anode with 3D transient models (Ref 1-3), the dispersion of particles at the injector exit, the perturbation of the plasma flow by the powder carrier gas flow, and the effect of plasma fluctuations on particle treatment. Unfortunately, these sophisticated codes have a long computing time which is not compatible with industrial needs. So, many simplified models have been or are developed which give good trends quickly for industrial applications.

This article presents the modeling with the ''Back Pressure'' model of phase change in a particle injected within a d.c. plasma jet. It is based on the Stefan problem (Ref 4) with an explicit determination of the position of the solid/liquid or liquid/gas interfaces. The developed model allows rather fast calculations (10 s with PC under Windows XP) compared to those obtained when using an enthalpy model of the phase change (Ref 5) (about 1 h in the same conditions).

This article was originally published in *Global Coating Solutions, Proceedings of the 2007 International Thermal Spray Conference*, Beijing, China, May 14-16, 2007, Basil R. Marple, Margaret M. Hyland, Yuk-Chiu Lau, Chang-Jiu Li, Rogerio S. Lima, and Ghislain Montavon, Ed., ASM International, Materials Park, 2007.

F. Ben Ettouil, B. Pateyron, H. Ageorges, M. El Ganaoui, and **P. Fauchais,** SPCTS, University of Limoges, Limoges, France; and **O. Mazhorova**, Keldysh Institute of Applied Mathematics, Moscow, Russia. Contact e-mail: fadhel.ben@etu.unilim.fr.

2. Modeling

2.1 Plasma Modeling

Plasma jet calculation was made using the fast software ''Jets&Poudres'' (Ref 6), which is built on the ''GENral MIXing'' code (GENMIX) (Ref 7). It deals with two-dimensional parabolic flow for Reynolds numbers $Re > 20$ and Peclet number $Pe > 50$. It neglects the carrier gas flow-plasma flow interaction but the obtained trends are in

Symbol List

a	thermal accommodation coefficient, = 0.8
Bi	Biot number
c_p	specific heat at constant pressure, J kg^{-1} K^{-1}
c_v	specific heat at constant volume, J kg^{-1} K^{-1}
C_D	drag coefficient
d_p	particle diameter, m
f', f''	correction factors of drag coefficient
f_0, f_1, f_2	correction factor of Nusselt number
h	coefficient of heat transfer, W m^{-2} K^{-1}
$Kn = \frac{l}{d_p}$	Knudsen number
l	mean free path, m
L_{sl}	melting latent heat, J kg^{-1}
L_{lv}	boiling latent heat, J kg^{-1}
m	mass, kg
M	molar mass, kg $mole^{-1}$

$Ma = \frac{\text{gas velocity}}{\text{sound velocity}}$	Mach number
$Nu = \frac{hd}{\mu}$	Nusselt number
p	pressure, Pa
$\text{Pe} = dp\rho cp/\kappa$	Peclet number
$\text{Pr} = \frac{\mu c_p}{\kappa}$	Prandtl number
r	particle radius, m
R	ideal gas constant = 8.314, J mol^{-1} K^{-1}
Re $= \rho(v_\infty - v_p)d/\mu$	Reynolds number
T	temperature, K
T_a	room temperature, K
u	velocity of vapor, m s^{-1}
v	velocity, m s^{-1}
$v_T = \sqrt{\frac{8RT_s}{\pi M}}$	mean molecular speed, m s^{-1}
ϑ_{sl}	velocity of the melting front, m s^{-1}
ϑ_{lv}	velocity of the vaporization front, m s^{-1}
$\gamma = \frac{c_p}{c_v}$	ratio of heat capacities
κ	thermal conductivity, W m^{-1} K^{-1}
μ	molecular viscosity, Pa s
ρ	mass density kg m^{-3}
σ	Stefan-Boltzmann constant = 5.67 × 10^{-8}, W m^{-2} K^{-4}

Indices

eb	ebullition
l	liquid
p	particle
sat	saturation
s	solid
v	vapor
∞	plasma

good agreement with those obtained with 3D sophisticated code (Ref 7) provided the carrier gas mass flow rate is below 1/6th of that of the plasma forming gas for standard injectors with internal diameter of 1.5-2 mm. Figure 1 illustrates the temperature field of the d.c. plasma jet and the zirconia particle (dp = 25 μm) trajectory under the operating conditions and used in the following, summarized in Table 1. This cartography makes it possible to distinguish three different areas within the jet (Fig. 1):

- *First region*: it corresponds to the plasma jet core, i.e. the hottest zone which extends about 40 mm downstream of the nozzle exit and in which the ambient penetration still low,

Table 1 Working conditions

Plasma gas	H_2-Ar 75% vol.
Nozzle internal diameter	7 mm
Plasma gas flow rate	60 L/min
Spray distance	100 mm
Surrounding atmosphere	Air
Electric power	32 kW
Thermal efficiency	57%
Effective thermal power	18,240 W

- *Second region*: it acts as the transition zone toward the turbulence marked by the fast decrease of the plasma temperature because of the penetration of the ambient air within the jet.
- *Third region*: it is where the temperature keeps decreasing as the plasma gas mixes more and more with the surrounding air.

2.2 Particle Dynamic Modeling

The trajectory of a single particle in the plasma jet is calculated starting from the balance of forces exerted on it: generally only drag and gravity forces are considered the other forces being neglected (Ref 8). The momentum equation is written as follows:

$$m_p \frac{dv}{dt} = \frac{1}{2} C_D \pi \frac{d_p}{4} \rho_\infty |v_\infty - v_p|(v_\infty - v_p) + m_p g. \quad \text{(Eq 1)}$$

The drastic gradients of temperature and gas properties within the thermal boundary layer surrounding the particle are taken into account by introducing corrective coefficients to the drag coefficient:

$$C_D = \frac{24}{\text{Re}}(1 + 0.11\text{Re}^{0.81}) f' f'' \quad \text{(Eq 2)}$$

where f' is the corrective coefficient suggested by Lee (Ref 9) to take into account the temperature variation within the boundary layer and f'' is the corrective factor corresponding to the Knudsen effect (Ref 10) which is not negligible for particles with dp < 10 μm.

$$f' = \left(\frac{\rho_\infty \mu_\infty}{\rho_\infty \mu_\infty}\right)^{0.45} \quad \text{(Eq 3)}$$

$$f'' = \left[1 + \left(\frac{2-a}{a}\right)\left(\frac{\gamma}{\gamma+1}\right)\frac{4Kn}{\text{Pr}}\right]^{-0.45} \quad \text{(Eq 4)}$$

2.3 Particle Heat Treatment Modeling

To deal with the heat treatment of particles under plasma conditions, the equation of continuity of the thermal flow, adapted to the spherical geometry is considered:

$$\rho_p c_{p,p} \frac{\partial T}{\partial t} = \frac{1}{r^2}\frac{\partial}{\partial r}\left(r^2 \kappa_p \frac{\partial T}{\partial r}\right). \quad \text{(Eq 5)}$$

The coefficient of heat transfer h is written as follows:

$$h = \frac{Nu\overline{\kappa}}{d_p}. \quad \text{(Eq 6)}$$

The thermal conductivity is given by the integrated expression proposed by Bourdin et al. (Ref 11):

$$\overline{\kappa}(T) = \frac{1}{T - T_a}\int_{T_a}^{T} \kappa(\theta) d\theta. \quad \text{(Eq 7)}$$

And the following Nusselt number has been considered:

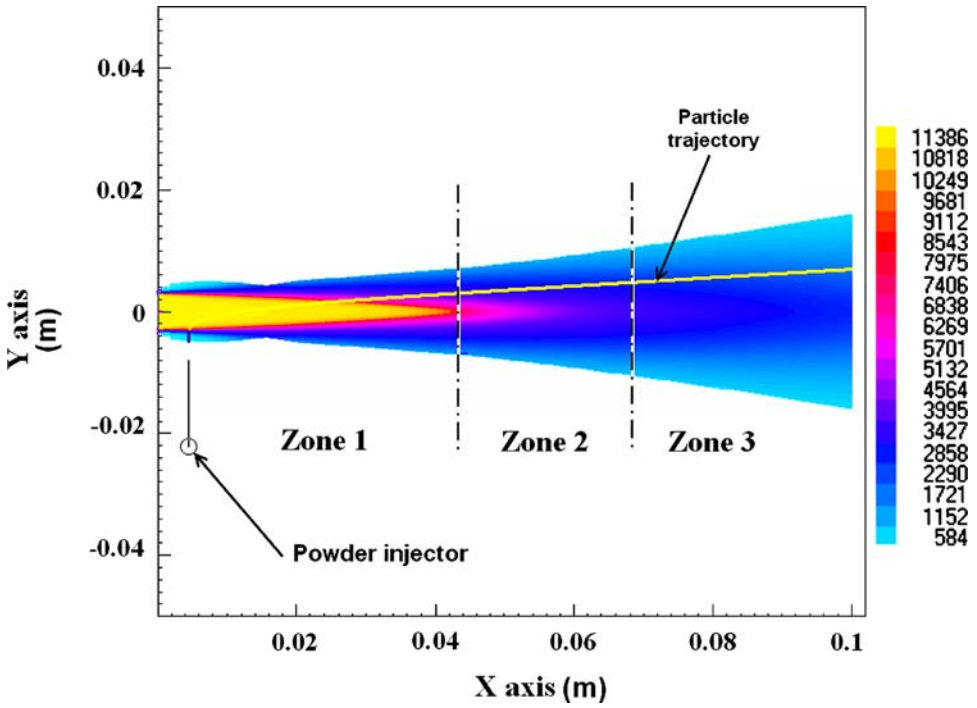

Fig. 1 Temperature fields and trajectory of a zirconia particle (d_p = 30 μm) in the plasma jet

$$Nu = \left(2 + 0.6\mathrm{Re}_p^{0.5}\,\mathrm{Pr}_p^{0.33}\right) f_0 f_1 f_2, \qquad \text{(Eq 8)}$$

where f_0, f_1, and f_2 are, respectively, the corrective factors related to the temperature variation in the boundary layer, the Knudsen effect and the vapor buffer around the particles (Ref 8-10).

$$f_0 = \left(\frac{c_p T_\infty}{c_p T_p}\right)^{0.38} \qquad \text{(Eq 9)}$$

$$f_1 = \left[1 + \left(\frac{2-a}{a}\right)\left(\frac{\gamma}{\gamma+1}\right)\frac{4Kn}{\mathrm{Pr}}\right]^{-1} \qquad \text{(Eq 10)}$$

$$f_2 = \frac{\dot{m}_v c_{p,\infty}}{d_p \pi \overline{\kappa}}\left[\mathrm{Exp}\left(\frac{\dot{m}_v c_{p,\infty}}{d_p \pi \overline{\kappa}}\right) - 1\right]^{-1} \qquad \text{(Eq 11)}$$

The progression of the solid-liquid interface is governed by the following equation:

$$\kappa_s \left.\frac{\partial T}{\partial r}\right|_{-} - \kappa_l \left.\frac{\partial T}{\partial r}\right|_{+} = \rho_l L_{sl} \vartheta_{sl}. \qquad \text{(Eq 12)}$$

The result of J. C. Knight (Ref 12) has been used to uncouple the calculations of the particle evaporation and from dynamic behavior. It relates the mass fraction of the flow leaving the Knudsen layer to the Mach number in air. The advance of the evaporation front is deduced from the mass conservation expressed by the equation:

$$\rho_l \vartheta_{lv} = \rho_v (\vartheta_{lv} - u). \qquad \text{(Eq 13)}$$

The velocity of the vaporization front can be written as follows:

$$\vartheta_{lv} = \frac{\rho_v u}{(\rho_v - \rho_l)} = W_{fr}\frac{\rho_{sat}\sqrt{RT/M}}{\sqrt{2\pi}}\frac{1}{(\rho_v - \rho_l)} \qquad \text{(Eq 14)}$$

where W_{fr} is the mass fraction leaving the particle through the Knudsen layer (the adjacent field to the particle) and described by the continuous averaged equation:

$$W_{fr} = \frac{\rho_v u}{\rho_{sat}\sqrt{RT/2\pi M}}. \qquad \text{(Eq 15)}$$

Given the approximation $\rho_v \ll \rho_l$ and the equation of state of ideal gases $p_{sat} = \rho_{sat} RT/M$, Eq 14 can be written as follows:

$$\vartheta_{lv} = -\frac{W_{fr}}{\rho_l}\frac{\rho_{sat}\sqrt{RT/M}}{\sqrt{2\pi}} = -\frac{1}{\sqrt{2\pi}}\frac{W_{fr}}{\rho_l}\frac{p_{sat}}{\sqrt{RT/M}}. \qquad \text{(Eq 16)}$$

The saturated vapor pressure p_{sat} at temperature T is given by:

$$p_{sat} = p_{eb}\exp\left[\frac{ML_{lv}}{RT_{eb}}\left(1 - \frac{T_{eb}}{T}\right)\right]. \qquad \text{(Eq 17)}$$

The problem of moving interfaces is treated, without using the enthalpy model. Previous equations are integrated with an implicit scheme of finished differences in an adaptive grid, in which the positions of different phase change fronts are fixed. The transformation coordinate depends only on interface velocities.

3. Results

3.1 Comparison of Dense Zirconia and Iron Particles

To illustrate the model developed, calculations are made for zirconia and iron particles, sprayed with an Ar-H2 d.c. plasma jet which characteristics are summarized in Table 1. Physical properties of the tested materials are summarized in Table 2. Injection velocities of particles with different sizes and/or specific masses are adjusted so that they follow the same trajectory, making an angle of about 4° with the jet axis, within the plasma jet.

Figures 2 and 3 show, respectively, the axial evolutions of the surface and center temperatures, along their trajectories, of zirconia and iron particles of 30 μm in diameter. For the iron particle, the variation in temperature between its surface and center is almost negligible, whereas a large temperature difference is developed in the zirconia particle between its surface and center as boiling starts at its surface while the temperature of its center is still close to the melting temperature which reaches that of the surface only at almost half of the stand-off distance, i.e., at $x \approx 50$ mm. The lumped model (uniform temperature in the particle) seems to be a good approximation in the case of metal particles, such as iron, with a good thermal conductivity compared to that of the plasma ($Bi < 0.01$), but it is not valid with ceramic materials, characterized by a poor thermal conductivity with $Bi > 0.03$.

The next figure confirms this result. In Fig. 4, the transient temperature distribution along the particle radius shows that the surface temperature of the zirconia particle increases quickly, on the contrary to its center temperature and thus the temperature gradient developed within the particle can reach 2650 K when surface starts melting. It is only at the end of the heat treatment in the plasma jet that both particle surface and center temperatures become close together with a difference of 300 K.

In the case of iron particle (the transient temperature being not presented here), the temperature gradient does not exceed 600 K at any time during its flight within the plasma jet. It takes only 128 μs to completely melt the iron particle against 225 μs for the zirconia particle.

Table 2 Physical properties of the tested materials

Physical properties	Dense ZrO_2	Porous ZrO_2	Iron
Mass density, kg m^{-3}	5680	2840	7960
Molar mass, kg $mole^{-1}$	123.22	123.22	55.84
Solid specific heat, J kg^{-1} K^{-1}	604	604	448.96
Liquid specific heat, J kg^{-1} K^{-1}	1387	1387	929
Solid thermal conductivity, W m^{-1} K^{-1}	1.66	0.55	16.3
Liquid thermal conductivity, W m^{-1} K^{-1}	5	5	16.3
Melting point, K			
Boiling point, K	2983	2983	1809
Melting latent heat, J kg^{-1}	4700	4700	3155
Boiling latent heat, J kg^{-1}	707×10^3 9×10^6	707×10^3 9.0×10^6	272×10^3 6.1×10^6

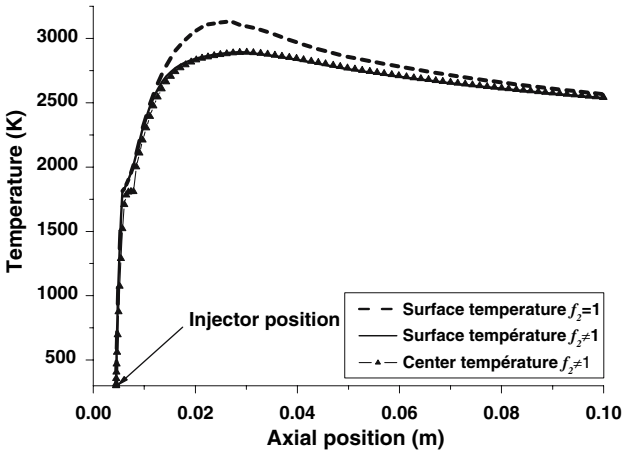

Fig. 3 Axial evolution of iron particle temperature ($d_p = 30$ μm)

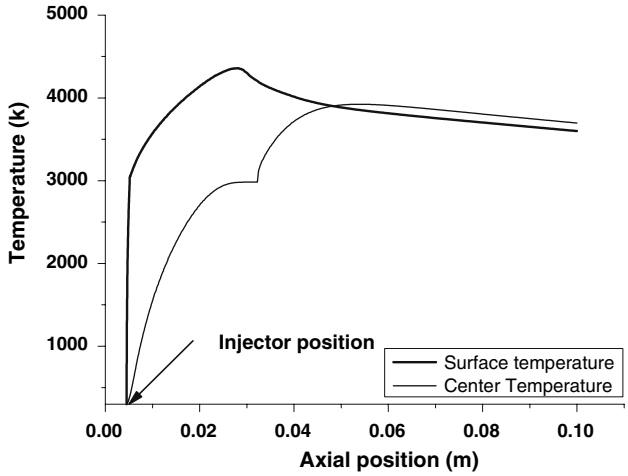

Fig. 2 Axial evolution of zirconia particle temperature ($d_p = 30$ μm)

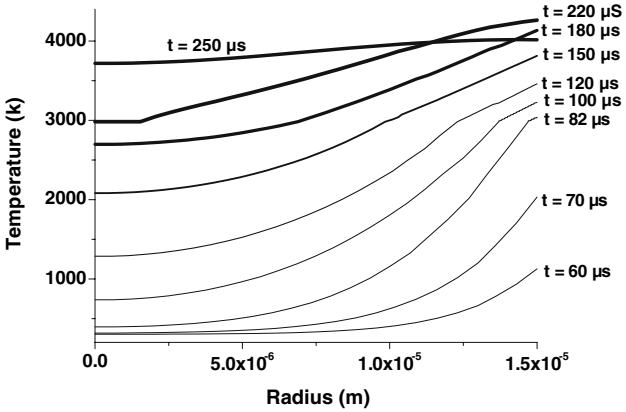

Fig. 4 Transient temperature distribution in a zirconia particle ($d_p = 30$ μm)

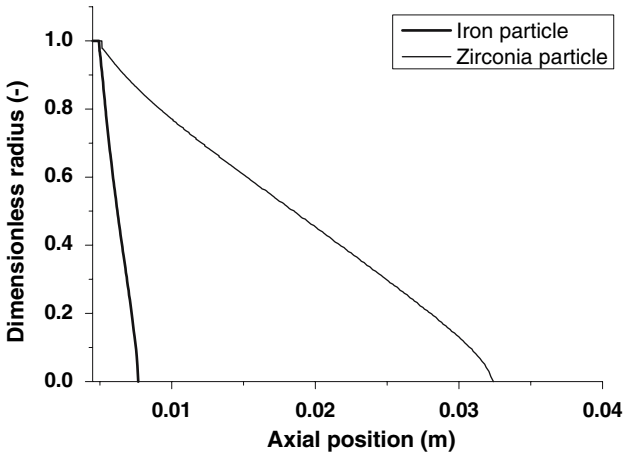

Fig. 5 Axial evolution of melting front

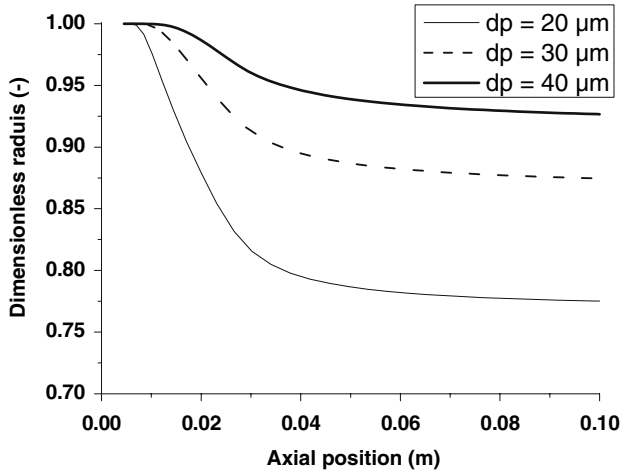

Fig. 6 Axial evolution of evaporation front in iron particles

Figure 5 illustrates the evolution of the melting front for both particles (zirconia and iron). Here again the thermal properties of the particles drive their behaviors, explaining why the iron particle melts completely after a trajectory of 5 mm in the jet, whereas the zirconia particle takes a distance six times longer distance in the jet to melt completely.

Figure 6 shows the evaporation front position (dimensionless radius) for three different particles diameter. An expected the evaporation is the most drastic for the smallest particle. It reaches 77% at the stand-off distance.

Figure 7 shows the evolution, along the axial position, of the mass lost by evaporation for iron particles of different diameters. Evaporation starts early with the smallest particle and it has to be noted that this loss increases abruptly at the beginning of evaporation (in the plasma jet core) and decreases as soon as the particle passes from the hot zones toward the cold zones of plasma. This rate increases with the size of the particles, and thus with their surface areas through which heat transfer from the plasma occurs.

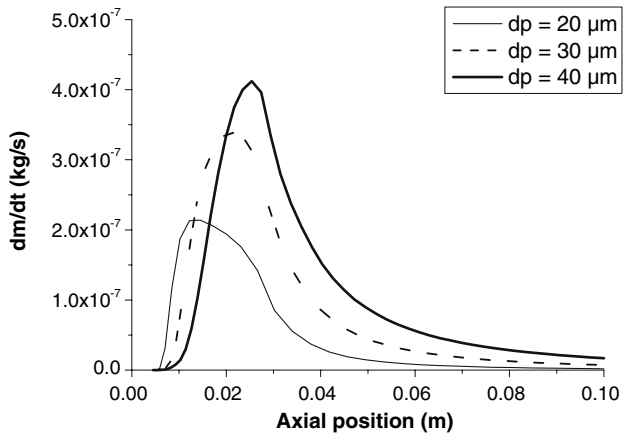

Fig. 7 Axial evolution of mass loss by evaporation for iron particles of different diameters

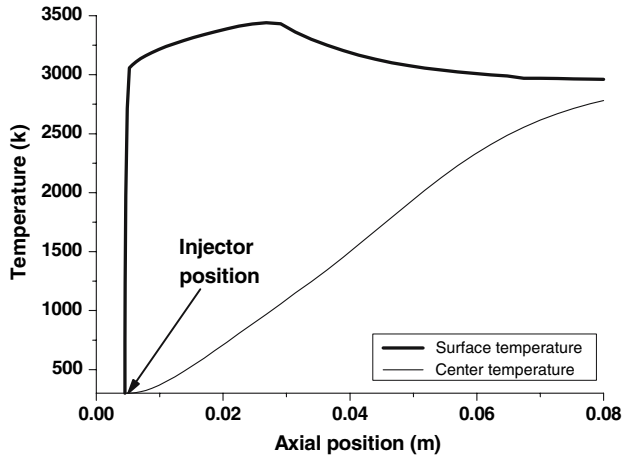

Fig. 8 Axial evolution of agglomerated zirconia particle temperature ($d_p = 45$ µm)

3.2 Spraying Agglomerated Zirconia Particles Made of Nanosized Particles

The plasma spraying of agglomerated particles aims at building partially nanostructured coatings (Ref 13). Particles must be only partially melted to keep their nanostructured core. The model has been adapted to the calculation of thermal and dynamic histories of nanostructured particles by taking into account the variation of particle characteristics (diameter, volume, area, etc.) due to the loss of porosity.

Figures 8 and 9 present the axial evolutions of the surface and center temperatures of nanostructured zirconia particles of respective diameters of 45 and 30 µm for a spray distance of 8 cm. Both trajectories were optimized through the injection velocity and particle properties as given in Table 2. The larger zirconia, particle impacts the substrate still with a solid core since the center temperature does not reach the melting point, which favors obtaining partially nanostructured coatings. At the opposite, the particle of 30 µm diameter is heated beyond the melting point and the nanostructured state is ruined.

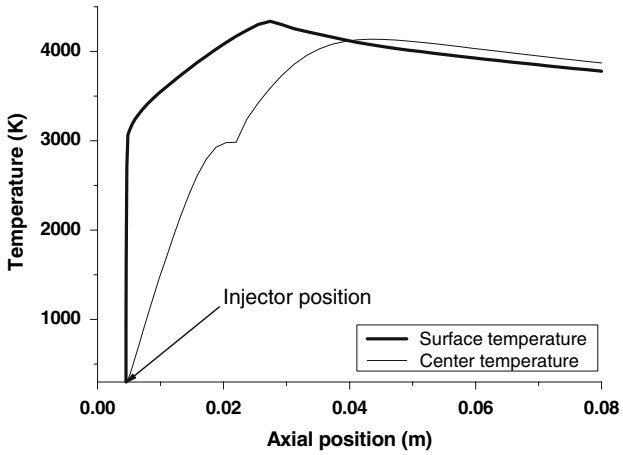

Fig. 9 Axial evolution agglomerated zirconia particle temperature ($d_p = 30$ μm)

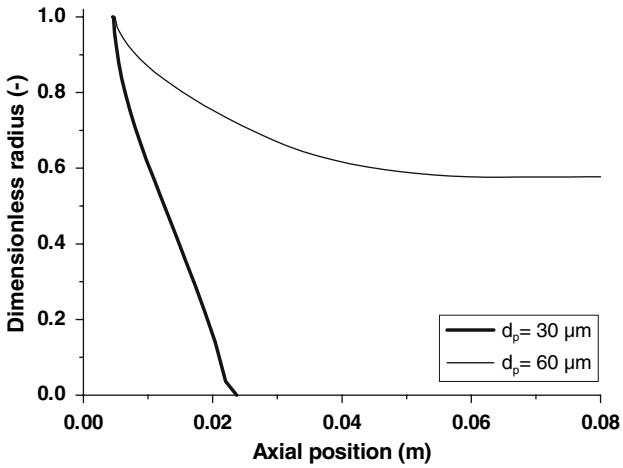

Fig. 10 Axial evolution of the melting front in agglomerated zirconia particles

The evolution of the melting fronts in these two particles (45 and 30 μm) is presented in Fig. 10, permitting the evaluation of the diameter of the nanostructured core (about 10 μm) in the large particle case and confirms the total melting in the small particle case.

Figure 11 presents the axial evolution of the melting fronts in agglomerated zirconia particle 50 μm in diameter, with two different injection velocities, the optimum velocity being 21 m/s. The evolution is the same in the first half of the trajectory. With the highest injection velocity, the porous zirconia particle crosses the plasma jet core and stays less time in the hottest plasma zone, so the unmelted particle core is larger than that with the optimum injection velocity.

4. Conclusions

A model dealing with thermal and dynamic behaviors of particles within stationary d.c. plasma jet has been

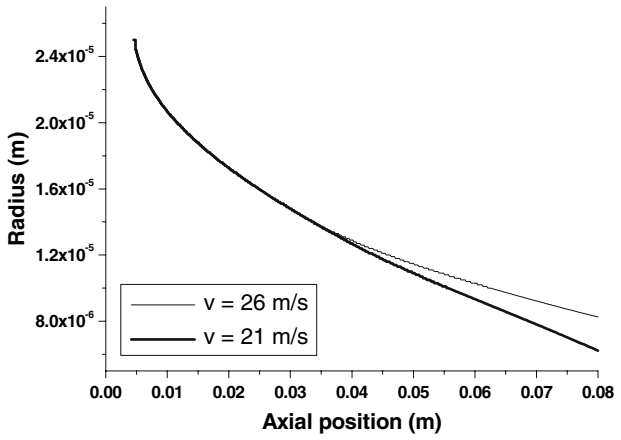

Fig. 11 Axial evolution of the melting front in agglomerated zirconia particle ($d_p = 50$ μm)

developed. Phase changes are taken into account by a finite difference scheme and simultaneous moving boundary layers between them. This model presents the advantage of a drastic low cost of calculation time, (10 s with PC under Windows XP) compared to an enthalpy model of the phase change (Ref 5) (about 1 h in the same condition).

This new model permits to investigate the influence of the spray working conditions and particle thermal properties on their melting and/or evaporation. Calculations for iron and zirconia particles show that phase change velocity is much slower in a low thermal conductivity particle, which develops a large difference between the surface and center temperatures.

Calculation for agglomerated nanosized particles permits the optimization of particle injection condition that promotes an unmelted agglomerated core keeping its initial nanostructure.

References

1. H.P. Li, E. Pfender, and X. Chen, Application of Steenbeck's Minimum Principle for Three-dimensional Modeling of DC Arc Plasma Torches, *J. Phys. D: Appl. Phys.*, 2003, **36**, p 1084-1096
2. P. Freton, J.J. Gonzalez, and A. Gleizes, Comparison Between a Two- and Three-Dimensional Arc Plasma Configuration, *J. Phys. D: Appl. Phys.*, 2000, **33**, p 2442-2452
3. C. Baudry, Contribution to the Transient and 3D Modeling of the Dynamic Behavior of the Arc within a Plasma Spray Torch, Ph.D. thesis, Univ. of Limoges, 2003
4. V. Alexiades and D. Solomon, Mathematical Modeling of Melting and Freezing Process, Hemisphere Publishing Corporation, USA, 1993
5. M. Bouneder, Modélisation des Transfert de Chaleur et de Masse dans les Poudres Composites Métal/Céramique en Projection Thermique, Ph.D. Thesis, Limoges University, 2006 (in French)
6. B. Pateyron et al., Jets & Powders Software (www.unilim.fr/spcts), 2007
7. G. Delluc, H. Ageorges, B. Pateyron, and P. Fauchais, Fast Modeling of Plasma Jet and Particle Behaviors in spray conditions, *High Temp. Mat. Process.*, 2005, **9**, p 211-226
8. E. Pfender, Particle Behaviour in Thermal Plasma, *Plasma Chem. Plasma Proc.*, 1989, **9**(1), p 167S-194S
9. Y.C. Lee, C. Hsu, and E. Pfender, Modelling of Particle Injection into a D.C Plasma Jet, *5th International Symposium on Plasma Chemistry, Edinburgh, Scotland*, Vol. 2, 1981, p 795-801

10. X. Chen, Heat and Momentum Transfer Between Thermal Plasma and Suspended Particles for Different Knudsen Numbers, *Thin Solid Films*, 1999, **345**, p 140-145
11. E. Bourdin, P. Fauchais, and M. Boulos, Transient Heat Conduction Under Plasma Condition, *Int. J. Heat Mass Transfer.*, 1983, **26**(4), p 582-652
12. C.J. Knight, Theoretical Modeling of Rapid Surface Vaporization with Back Pressure, *AIAA J.*, 1979, **17**(5), p 519-523
13. R.S. Lima, A. Kucuk, and C. Berndt, Bimodal Distribution of Mechanical Properties on Plasma Sprayed Nanostructured Partially Stabilized Zirconia, *Mat. Sci. Eng.*, 2002, **A327**, p 224-232